Nuclear Instruments and Methods in Physics Research A 1070 (2025) 170001

Contents lists available at ScienceDirect

Nuclear Inst. and Methods in Physics Research, A

journal homepage: www.elsevier.com/locate/nima

Full Length Article

New readout system of the FATIMA detectors based on Silicon Photomultipliers arrays

S. Pascu [a,b,*], A. Stoica [b,c,**], C. Neacşu [b], A. Bruce [d], C. Costache [b], B. Das [e], M. Górska [e], C. Mihai [b], M. Mikolajczuk [e,f], Zs. Podolyák [a], P.H. Regan [a,g], A. Turturică [b]

[a] School of Mathematics and Physics, University of Surrey, Guildford, GU2 7XH, United Kingdom
[b] National Institute for Physics and Nuclear Engineering, Bucharest-Magurele, R-77125, Romania
[c] Physics Department, University "Politehnica" of Bucharest, Bucharest, Romania
[d] School of Computing Engineering and Mathematics, University of Brighton, Brighton, BN2 4GJ, United Kingdom
[e] GSI Helmholtzzentrum fuer Schwerionenforschung GmbH, Darmstadt, 64291, Germany
[f] Faculty of Physics, University of Warsaw, Warsaw, 02-093, Poland
[g] Marine, Medical and Nuclear Department, National Physical Laboratory, Teddington, TW11 0LW, United Kingdom

ARTICLE INFO

Keywords:
SiPM
PMT
$LaBr_3$(Ce) scintillator
FATIMA
Fast-timing

ABSTRACT

We present a new readout system based on large area Silicon Photomultipliers arrays coupled with cylindrical 1.5" × 2" $LaBr_3$(Ce) FATIMA-type crystals. This readout achieves the fast-timing capabilities of such crystals coupled to the usual Photomultiplier Tubes. Energy calibration was measured with ^{137}Cs and ^{152}Eu standard radioactive sources, while the timing performances were investigated with a ^{60}Co radioactive source. We benchmark our results against the corresponding results obtained with the fast R9779 Photomultiplier tubes and highlight the importance of achieving similar energy and timing performances for nuclear structure experiments. The FWHM energy resolution for the 1.5" × 2" $LaBr_3$(Ce) crystal coupled with the SiPM and PMT was found to be 3.31(2)% and 3.85(1)%, respectively, for the 661.6 keV transition of the ^{137}Cs source. The timing resolution was measured between a conical crystal known for its fast response and a cylindrical crystal coupled to a SiPM or PMT readout. We obtain values of FWHM = 230(1) ps and 232(1) ps, respectively, between the 1173.2–1332.5 keV transitions of the^{60}Co source. In addition, a temperature effect compensation circuit was developed to maintain a good stability of the gain during long measurements, typical for in-beam/off-beam experiments in nuclear physics.

1. Introduction

Photon detection technology plays a pivotal role in various scientific fields, ranging from fundamental research in particle physics to medical imaging and environmental monitoring. Among the many photon detection devices available, Silicon Photomultipliers (SiPMs) and Photomultiplier Tubes (PMTs) stand out as two prominent players. Both devices excel in detecting low-level light signals with exceptional sensitivity, yet they differ significantly in their operational principles, performance characteristics, and application scopes.

In recent years, the rapid advancement of semiconductor technology has led to the emergence of SiPMs [1,2] as a promising alternative to the well-established PMTs. SiPMs, also known as silicon avalanche photodiodes (APDs), offer several advantages over traditional PMTs, including compact size, low operating voltage, insensitivity to magnetic fields, and good timing resolution. These qualities make SiPMs particularly attractive for applications where space constraints, power consumption, and timing precision are critical factors. As such, they have been used in fields like γ-ray spectroscopy [3], medical applications [4], astrophysics [5], environmental monitoring [6], and homeland security [7].

Conversely, PMTs have been the workhorse of photon detection for decades, renowned for their high gain, low noise, wide spectral response, and large active area. Their robustness and versatility have rendered them indispensable in numerous scientific experiments and industrial applications. However, PMTs suffer from certain limitations, such as high voltage requirements, susceptibility to magnetic fields, and bulky size, which have stimulated interest in exploring alternative technologies like SiPMs [8].

In nuclear spectroscopy, one of the most simple and reliable methods for the half-life determination of excited states of atomic nuclei

* Corresponding author at: National Institute for Physics and Nuclear Engineering, Bucharest-Magurele, R-77125, Romania.
** Corresponding author.
E-mail addresses: sorin.pascu@nipne.ro (S. Pascu), alexandru.stoica@nipne.ro (A. Stoica).

https://doi.org/10.1016/j.nima.2024.170001
Received 10 July 2024; Received in revised form 8 October 2024; Accepted 18 October 2024
Available online 24 October 2024

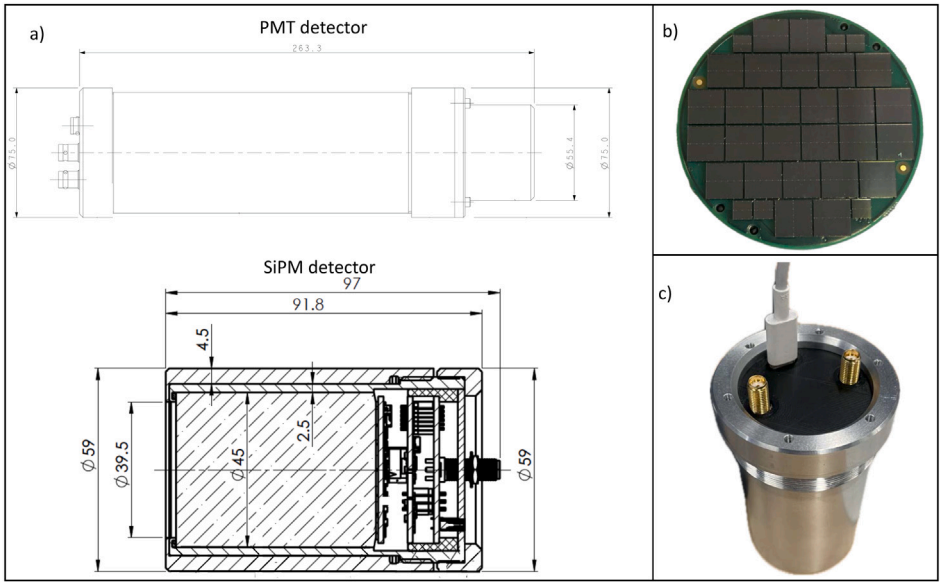

Fig. 1. (a) Mechanical design of the aluminum casings for the PMT- (upper part) and SiPM-based detector (lower part). The SiPM and the associated electronics are packed in a more compact configuration with respect to the size of the PMT; (b) View of the circular SiPM array with a diameter of 1.5"; (c) View of the SiPM detector placed inside an aluminum casing.

is called "fast-timing". The method covers a broad range of half-lives, typically from nanoseconds down to the picoseconds region [9,10]. The technique relies on the fast response of the detector to select the time difference between two γ rays, one populating and the other one de-exciting the level of interest. The use of $LaBr_3$(Ce) crystals, offering superior energy resolution, faster decay time, and higher light yield compared to traditional scintillation materials, has revived the interest for this method [11,12].

The FAst TIMing Array (FATIMA) [13] detector system was developed for the DEcay SPECtroscopy (DESPEC) [14,15] experiment at FAIR (Facility for Antiproton and Ion Research). It currently consists of 36 $LaBr_3$(Ce) crystals with a diameter × length = 1.5" × 2", coupled to fast R9779 Hamamatsu PMTs. It allows for half-life measurements with the $\gamma - \gamma$ fast timing method down to a few picoseconds. Similar to FATIMA, several other detector setups dedicated to fast-timing measurements use a $LaBr_3$(Ce) or a $CeBr_3$ combination of a scintillating crystal coupled to a PMT [16–18]. Despite the growing interest in SiPMs, all the experimental investigations performed so far with this method have used the combination of a crystal coupled to PMTs (see, for example, Ref. [13] and references therein). According to our knowledge, such attempts have only been performed in [19,20]. The results showed for the first time that SiPMs can be an excellent alternative to PMTs for fast-timing measurements. However, the time resolutions reported in [19] were about 25% worse than the ones obtained with a PMT. Therefore, this article aims to build on the work in [19,20] and bridge this gap by providing an improved readout architecture and achieving, for the first time, similar timing resolutions for the two configurations.

The main components of the system architecture and the mechanical design are presented in Section 2. The experimental setup and the associated electronics are described in Section 3, while the results for the energy and timing resolutions, as well as for the temperature compensation circuit, are given in Section 4. By elucidating the strengths and limitations of SiPMs and PMTs with $LaBr_3$(Ce) crystals, this comparative analysis will contribute to the ongoing discourse surrounding photon detection technology, facilitating the adoption of optimal solutions across diverse scientific and industrial domains.

2. System architecture and mechanical design

One of the main advantages of using an array of SiPM cells arranged in a circular configuration is that the detection efficiency can be increased by placing the detectors in a compact geometry. The design of the FATIMA detectors was using a 1.5" × 2" $LaBr_3$(Ce) crystal coupled with a 2" × 2" R9779 Hamamatsu 8-stages PMT. In addition, the whole system was encapsulated in an aluminum case. The two structures are presented in Fig. 1 in panel (a). It is clear that the overall dimensions of the PMT-based detector are considerably larger than the size of the crystal. Therefore, an effort was made to design a more compact setup that was only slightly larger than the diameter of the crystal. In the first phase, a quasi-circular array of SiPM cells has been developed using a combination of 26 6 × 6 mm^2 and 6 3 × 3 mm^2 cells (see Fig. 1b), designed to follow the circular base of the cylindrical crystal while covering most of the $LaBr_3$(Ce) crystal surface. Using the combination

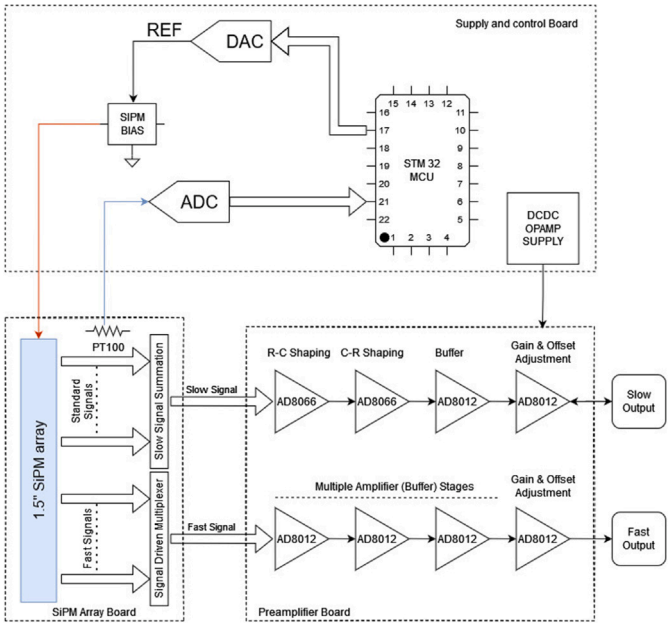

Fig. 2. Block diagram showing the system architecture for the readout of a 1.5" × 2" $LaBr_3$(Ce) crystal: (left) SiPM array board; (right) preamplifier board; (top) supply and control board.

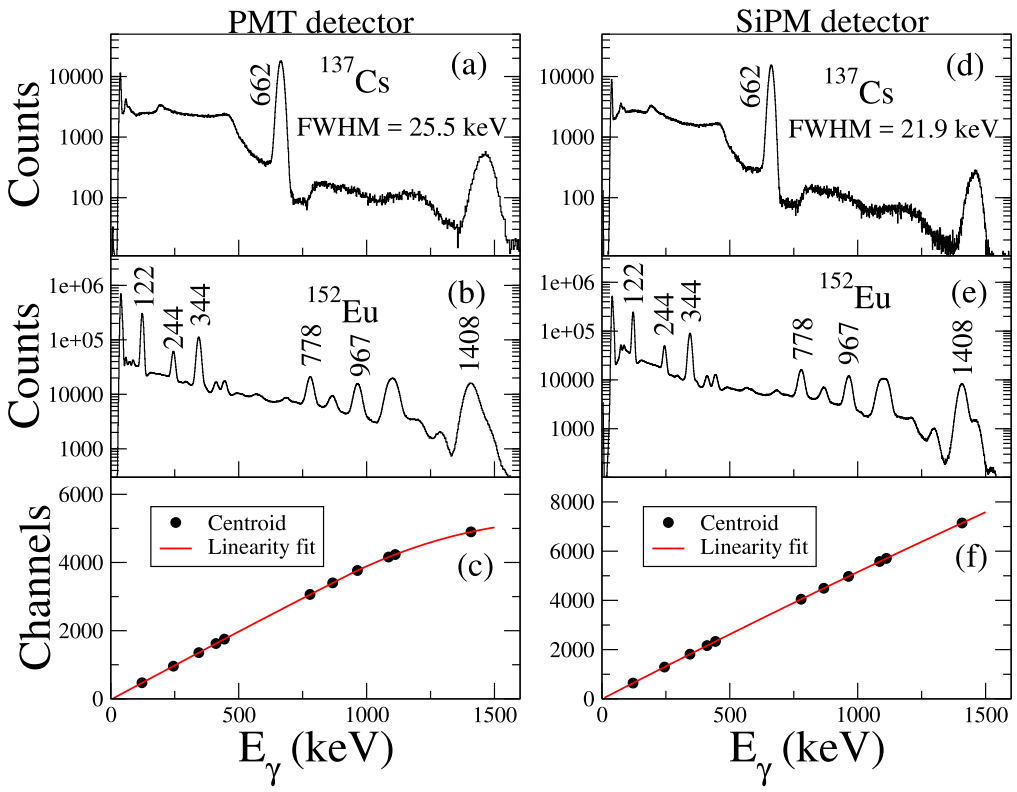

Fig. 3. γ ray spectra of ^{137}Cs (panels (a) and (d)) and ^{152}Eu sources (panels (b) and (e)) measured using the PMT detector (left) and SiPM detector (right). FWHM is indicated on the figure for the 662 keV transition of ^{137}Cs. A smaller value is obtained for the SiPM detector compared to the PMT detector. Panels (c) and (f): linearity plot for the two detectors, given as a function of peaks position (in channels) versus energy (in keV).

of small (3 × 3 mm^2) and large (6 × 6 mm^2) SiPM cells, as well as a more compact packing of the cells (0.1 mm between neighboring cells) as compared to the one reported in [19] with 0.32 mm between cells, we estimate the array covers about 86% of the crystal's area. The array is mounted on a circular Printed Circuit Board (PCB) (43 mm diameter), and all the electronic boards have a circular shape. In a second step, a new aluminum casing to accommodate the crystal and the readout electronic boards were developed, as shown in Fig. 1(c). The length of the detector is reduced by a factor of 2.7, while the diameter with about 20%.

The circular array is based on 6 × 6 mm^2 MicroFJ-60035-TSV-TR (35 μm microcell size) and 3 × 3 mm^2 MicroFJ-30020-TSV-TR (20 μm microcell size) J-Type SiPM cells from Onsemi [21] (former SensL). Each 6 × 6 mm^2 cell contains 22292 microcells, while the 3 × 3 mm^2 has 14410 microcells. A fill factor of 75% and 62% is achieved for each cell, with a photon detection efficiency of 50% and 38%, respectively. A high gain is obtained in each case, 6.3 × 10^6 and 1.9 × 10^6, with a dark current rate of 150 kHz/mm^2 and 125 kHz/mm^2, for the two cell types, respectively.

The most obvious way to read an array of SiPM cells would be to read each cell independently, providing a very good signal-to-noise ratio. However, several practical constraints may hinder the implementation of this approach, and in the case of applications where position sensitivity is not required, this method would result in a very high cost/performance ratio, doubled by large volume electronics and high power consumption and heating. An alternative approach is to use the multiplexing solution [22]. Various readout architectures exist to achieve this multiplexing, tailored to specific applications. The advantages of multiplexing include simplified complexity and reduced costs stemming from fewer electronic and data acquisition channels. The drawback is that the method might degrade the detector timing performance due to the high capacitance of SiPM sensors. In the present paper, a multiplexing method as described in Refs. [23,24] was implemented as a readout method. We show that the timing performances are not severely affected for the purpose of our application, and the resulting front-end electronics can be used with success for fast-timing measurements.

The block diagram of the system architecture is presented in Fig. 2, and it features three electronic boards. The first one is the SiPM array board, where the readout of the cells is performed. The method is similar to the one developed and tested in Ref. [19] and employs four individual groups. While the standard outputs are summed directly, the fast signals are collected using the method described in [19,23]. Having a positive and a negative outputs ensures a high compatibility with the experimental setup used traditionally for the PMT detectors, in particular for the use of the constant fraction discriminator (delay and zero crossing). The signals are then passed to the preamplifier board. The preamplifier is built with operational amplifiers (2 × AD8066 + 2 × AD8012 for the slow signal, and 4 × AD8012 for the fast signal) and allows the formation of the slow and fast outputs. The operational amplifiers are powered up from a DCDC converter, which in turn is powered up from the USB connector. This combination of operational amplifiers allows for reduced power consumption, as well as a relatively short fall time constant of ≈ 0.6 μs to avoid pileup effects. The maximum peak amplitude of the pulses is 1.7 V and 1.9 V, for the fast and slow signals, respectively, with a 50 Ω termination. The final stage is the supply and control board for gain-drift compensation. The signal from the PT100 sensor mounted on the SiPM board is read by 24-bit analog-to-digital converter (ADC) and a microcontroller is used to adjust the SiPM bias voltage relative to a temperature reference using a digital-to-analog converter (DAC).

3. Experimental setup

The experimental setup aimed at testing the SiPM assembly consisted of four $LaBr_3$(Ce) scintillating crystals of various shapes coupled to either PMTs or SiPMs. The first two detectors used height × diameter

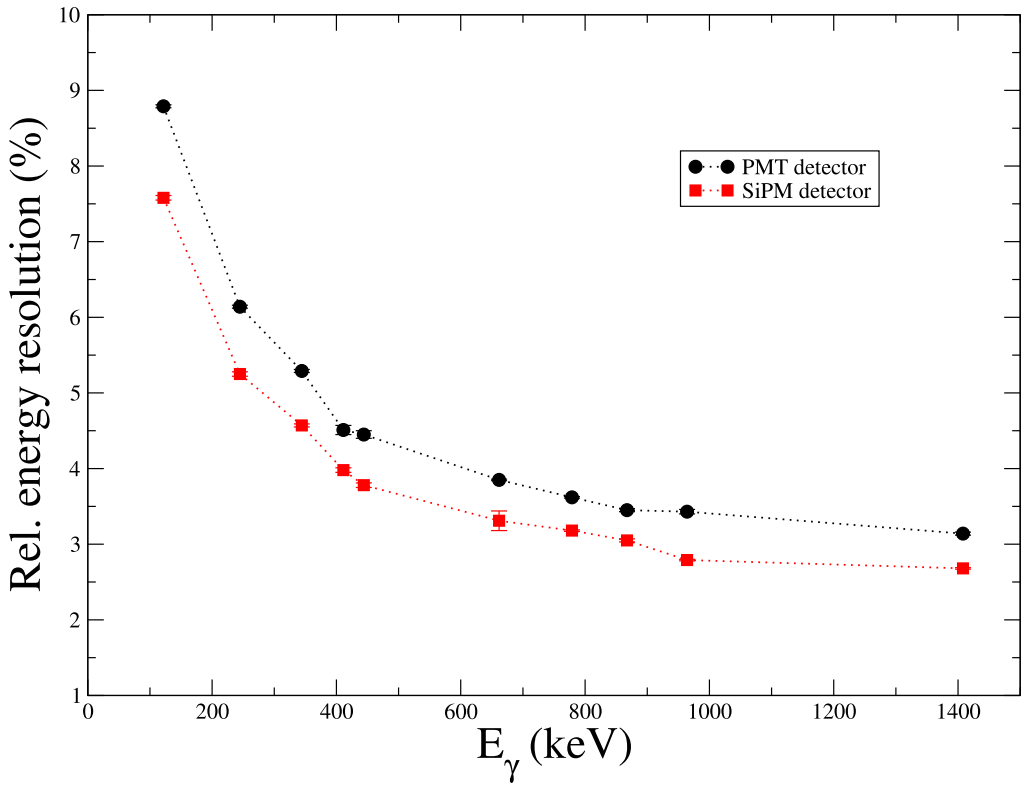

Fig. 4. Relative energy resolution (FWHM) up to 1.408 MeV transition of an ^{152}Eu radioactive source for the PMT (black) and SiPM (red) detectors. The SiPM performs better for a wide range of energies, up to 1.4 MeV.

at the base × diameter at the top = 1.5" × 1.5" × 1" conical-shaped crystals coupled to R9779 PMTs. They have a very fast and well-known response, and therefore, one of them was always used as a start for the timing measurements, as explained in Section 4.2. The third detector was a 1.5" × 2" cylindrical crystal coupled with the same R9779 PMT. This "classical" FATIMA-type detector was used to provide a reference measurement for the energy and timing capabilities of the FATIMA array. Finally, the fourth detector in the setup was a 1.5" × 2" cylindrical crystal coupled with the SiPM array developed in the present study. The detectors were positioned at an angle of 90° with respect to each other, while lead bricks were placed in between to avoid scattering of γ rays from one detector to another. The radioactive sources were placed in the middle of the setup. The typical distance between the detectors and the source was about 5 cm.

The conical detectors were biased at −1100 V, the cylindrical crystal coupled with the PMT at −1200 V, while the cylindrical crystal coupled to the SiPM array to 28 V. For the PMT-based detectors, we used the dynode signal for energy determination and the anode signal to obtain the timing information. For the SiPM detector, the standard signal was used for energy measurements, while the fast signal was used to obtain the timing resolutions. The energy signals (dynode and standard) were fed directly to a 14-bit 500 Ms/s DT5730 CAEN digitizer that used an integral algorithm to construct the spectra. An analog electronic system was used to process the negative signals of the detectors (anode and fast). The signals were fed first to an Ortec 935 quad CFD and processed with the usual constant fraction discriminator algorithm employed in fast-timing measurements. The logic output signal marks very precisely the time when a γ ray was registered by the detector. These signals were fed to three Ortec 567 TAC modules to obtain the time differences. The first conical detector was always used as a START, while the other three detectors were fed sequentially as STOP to each of the three TAC modules. The output signals of these modules were further fed to the DT5730 CAEN digitizer to form the time spectra.

Standard ^{137}Cs, ^{152}Eu radioactive sources were used for energy calibration, while a ^{60}Co source was used for time calibration. These results will be presented in the next section. To calibrate each of the three TAC modules for timing purposes, the signal of the first detector was used both as a START and as a STOP, with a Phillips 792 dual delay module inserted on the STOP path after the CFD. About ten calibration points were taken for each TAC module in steps of 0.5 ns. The time spectra will be presented and discussed in Section 4.2.

4. Results

4.1. Energy resolution

In this section, we present the comparison between a 1.5" × 2" cylindrical crystal coupled to the PMT or the SiPM (detectors 3 and 4, called PMT and SiPM detectors for short from now on). The spectra taken with ^{137}Cs and ^{152}Eu radioactive sources are shown in Fig. 3 panels (a) and (b), respectively, for the PMT detector, and in panels (d) and (e), for the SiPM detector. As the energy resolution of the $LaBr_3$(Ce) crystals is typically given by the manufacturers for the 662 keV transition of the ^{137}Cs, we first discuss this result. We obtain a full width at half maximum (FWHM) value of 21.9(1) keV (3.31(2)%) for the SiPM detector, in comparison with the 25.5(1) keV (3.85(1)%) for the PMT detector. This value is slightly worse than the one obtained in [19] with a different configuration of SiPM cells (3.1(1)(%)). We note that even better energy resolution can be obtained with other configurations, for both SiPM and PMT detectors, by using readout systems dedicated to energy resolution. For example, in Ref. [3], the authors have obtained a value of 2.6(%) at 662 keV using a 3" × 3" crystal and a dedicated SiPM array, as well as a Hamamatsu R6233 PMT. This was possible by reading all 144 SiPM cells individually with an ASIC, while in the case of the PMT result, a photomultiplier optimized for energy measurements was used. Our R9779 PMT is optimized for timing resolution and will consequently have worse properties for energy measurements.

The energy resolution of the SiPM detector is affected by the thermal drift of the SiPM cells. The present results have been obtained using the

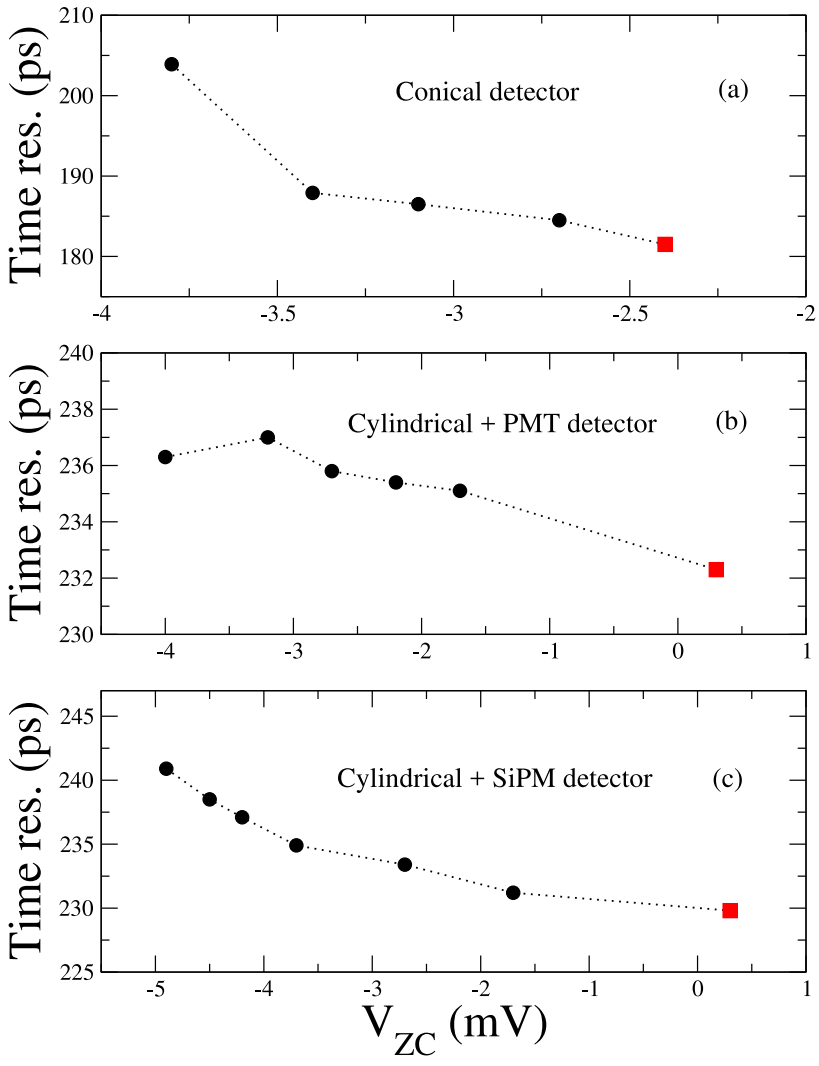

Fig. 5. Zero-crossing variation of the constant fraction module in search of the optimum timing resolution measured between the 1173–1332 keV transitions of the ^{60}Co source. The START signal was provided by the first conical detector in each case, while the stop is given by the other conical detector (panel (a)), the PMT detector (panel (b)), and the SIPM detector (panel (c)), respectively. The ZC was measured with respect to the ground connection of the CFD module. The optimum value is shown with a red square in each case.

thermal compensation circuit described in Section 4.3. Nevertheless, for practical purposes, we employed up to one-hour-long runs to minimize any effect due to thermal variations in the ambient environment. Aside from significant drifts of the SiPM gain in the first ≈30-40 min after power-up, we have not observed any significant drift during these short runs. Results from longer runs will be presented in the last subsection of this paper.

In Fig. 3, panels (c) and (f), we present the linearity plot of the PMT and SiPM detectors up to 1408 keV using the ^{152}Eu standard calibration source. With the current bias voltages used (28 V for SiPM and −1200 V for PMT), it is clear that the SiPM detector shows considerably less non-linear effects, while due to the high voltage used, the PMT detector starts to saturate around 1000 keV. We note that the spectra presented in Fig. 3 are calibrated with polynomials of different order. If the SiPM detector is rather linear up to 1.4 MeV (a second-degree polynomial is used with a small coefficient of the leading term), the PMT detector is calibrated separately on two distinct regions with second degree polynomials. Reducing the bias voltage will make the detector response more linear, but will considerably affect the timing performances.

In Fig. 4, we investigated the evolution of the FWHM obtained with the two detectors for a wider range of energies. We present results only up to 1.4 MeV for the single peaks which can be easily distinguished with the resolution of these detectors. For other transitions, the presence of multiple closed-lying transitions hampers a clear analysis. Our analysis found that the SiPM-based detector performs better than the PMT detector for energies up to 1.4 MeV.

4.2. Timing characteristics

This subsection presents the results obtained from the delayed coincidence measurements. As mentioned before, the first conical detector always acts as a START (the 1332 keV $2^+ \rightarrow 0^+$ transition in ^{60}Ni), while the other detectors provide the STOP signal (the 1173 keV $4^+ \rightarrow 2^+$ transition in ^{60}Ni) of each of the TAC modules. The timing resolution (FWHM) between two such detectors is known to be 178(4) ps [25]. Therefore, in order to know that the best CFD parameters are employed for the conical detector used as a start signal, in the first part we focused our attention on optimizing the timing resolution between the two conical detectors. Therefore, the delay and the zero-crossing (ZC) adjustment were used to define the timing characteristics of these detectors. For the conical detectors, a 1 ns delay was used in combination with a “no delay” and a “blocking mode” setting of the CFDs. These settings were set as jumpers inside the Ortec 935 quad CFD and were used for all four channels irrespective of the detector used. Keeping constant the 1 ns delay, we proceed to vary the zero-crossing

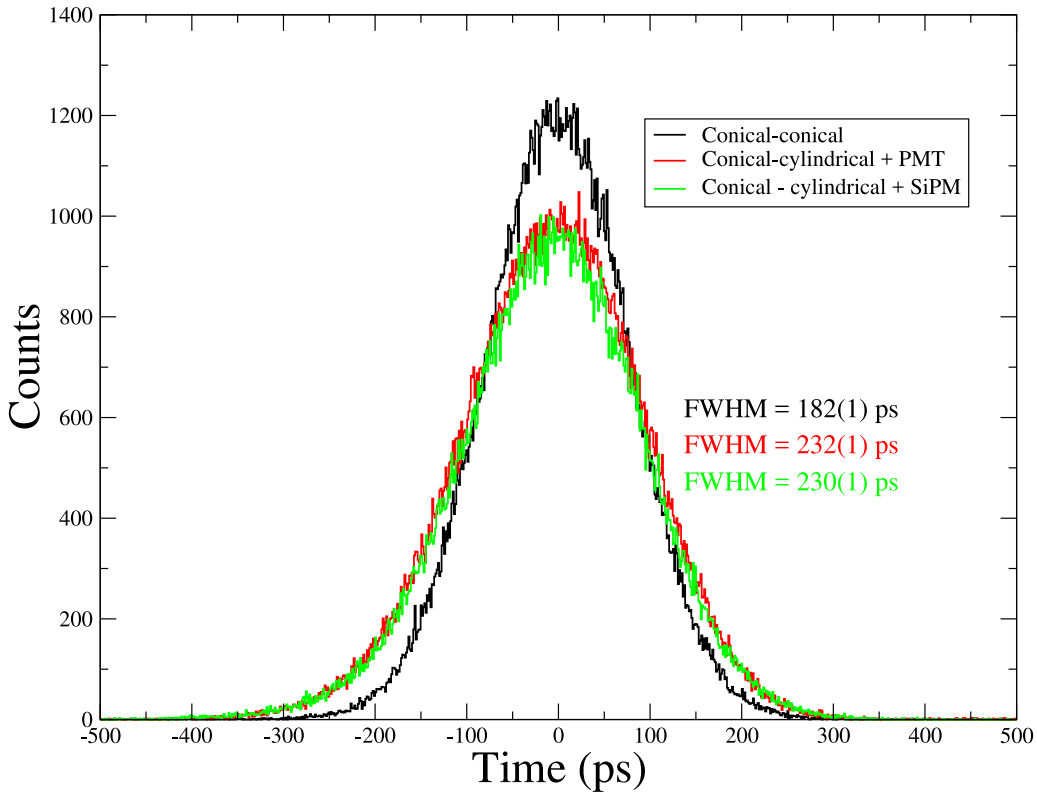

Fig. 6. Time distributions for the 1173–1332 keV transitions of ^{60}Co obtained with the conical detector used as a START signal and the other three detectors as a STOP signal: conical (black), cylindrical with PMT (red), and cylindrical coupled with SiPM (green). The two time distributions corresponding to the cylindrical detectors (red and green) are almost identical, demonstrating for the first time that the SiPM arrays are an efficient alternative to the PMTs.

setting of the CFD. For all the detectors, the zero-crossing is measured with respect to the ground connection of the module. The results of this analysis are presented in Fig. 5 panel (a). The minimum is obtained at −2.4 mV, and the timing resolution is measured to be 181(1) ps. This value is very close to the value measured in [25].

Having the start detector optimized for fast timing measurements, the timing characteristics of the cylindrical PMT detector were investigated in a second step. The timing resolution (FWHM) of such detectors is known to be around 210 ps [26]. As for the conical detectors, the delay was first varied, and a minimum was obtained for a delay of 2 ns. Subsequently, the zero-crossing was adjusted as presented in Fig. 5 panel (b). The minimum is found at 0.3 mV, and the timing resolution between the conical detector and the cylindrical PMT is measured to be 232(1) ps.

Finally, the same optimization procedure was employed for the SiPM detector. Due to the different shape of the signal (less steep rise time as compared to the PMT detector signal), a value of 5 ns was found as the optimum value. Variation of the zero crossing has yielded a value of 0.3 mV, as for the PMT detector (see Fig. 5 panel (c)). A time resolution of 230(1) ps is obtained, the same within the uncertainties as the one obtained for the PMT detector.

The optimized time spectra obtained in the current measurement for all three combinations of detectors are summarized in Fig. 6. It is clear that the SiPM detector performs at least as well as the PMT detector, making it a suitable candidate for use in fast-timing measurements. We note that the best time resolution obtained in [19] was about 277(2) ps, measured between a conical 1.5” × 1.5” × 1” and a 2” × 2” SiPM detector, in comparison with the 220(1) ps obtained with the same cylindrical detector coupled to a PMT. This significant difference of time resolution between the two cases is explained by: (i) the rectangular shape of the SiPM array used in that paper, which exceeds the area of the crystal, increasing the dark noise considerably; (ii) a larger rise time of the fast pulse. With the current circular design and a steeper rise time of the signal, we are able, for the first time, to achieve comparable time resolutions between the SiPM and PMT detectors.

4.3. Temperature compensation

The gain stability of the detectors is very important in γ-ray spectroscopy measurements. For experiments that require measuring for a long time, on the scales of weeks or sometimes even months, the temperature may vary considerably, affecting the stability of the gain and, consequently, the energy resolution. Therefore, we developed a gain-compensation circuit that can be used to correct this effect.

The origin of the gain variation with temperature stems from its dependency on the overvoltage ΔV and the junction capacitance C_{cell}. These variations were studied in detail in the case of several SiPM types in Ref. [27]. The authors found that the most significant contribution comes from the breakdown voltage dependence on temperature. In the case of the Onsemi (former SensL) cells, with an average slope of 18.9 mV/°C and for an overvoltage of 3 V, typical for the cells used in the present paper, the fractional change of the overvoltage is about 0.63% for each one-degree change in temperature. The junction capacitance has a much smaller contribution, with a change of only about 5% for the range of temperatures between −40° and +40°. This amounts to about 0.06% fractional change for each one-degree change in temperature. It is worth mentioning that, in addition to the breakdown voltage and the cell capacitance, the temperature also has an effect on the dark current rate. The dependency is exponential and can be attributed to changes in the thermal generation of charge carriers [27].

We have developed a custom biasing compensation module capable of handling the gain shifts due to temperature variations. From our measurements, we obtained a slightly different value for the gain slope with temperature of 25 mV/°C. The bias voltage of the SiPM matrix is obtained with a DCDC boost converter, powered with 5 V through

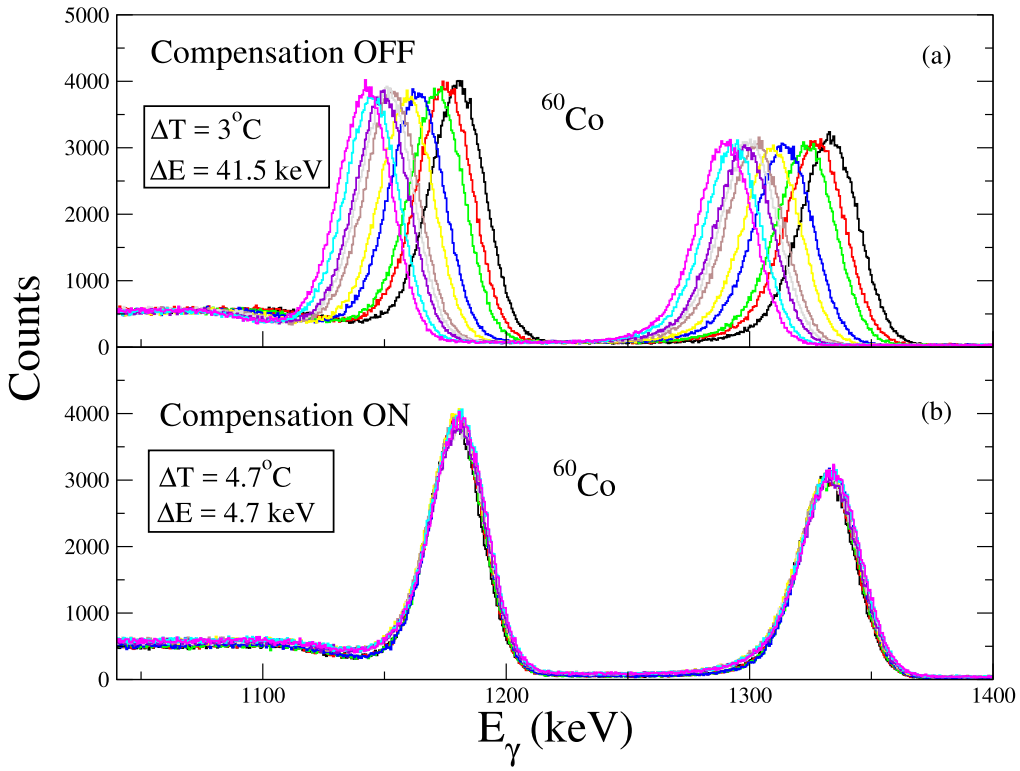

Fig. 7. Superposition of 10 energy spectra taken with a ^{60}Co source without (panel (a)) and with the temperature compensation circuit (panel (b)). The gain variation is measured to be 41.5 keV over a 3 °C temperature interval in the case of the uncompensated circuit, and it amounts to only 4.7 keV for a temperature variation of 4.7 °C in the case of the compensated circuit.

a USB type C connector. Temperature information is obtained from a 24-bit ADC, LTC2411, coupled to a PT100 sensor. An STM32L072KZ microcontroller (MCU) reads the temperature every second, calculates the required bias voltage, and adjusts it using a 16-bit DAC80501. A nominal voltage of 28 V was proven, nevertheless, to be an optimum value for obtaining good energy and timing resolutions, so the range in which the voltage can vary was chosen between 27.5 V and 28.5 V. The calibration parameters required for the SiPM bias DCDC source and the gain compensation slope are kept in the EEPROM memory of the MCU. They can be modified through a serial communication using the USB interface. The MCU can be programmed using the USB interface, making a software upgrade easy.

In Fig. 7, we present the results of the measurements with and without the temperature compensation circuit. The tests were performed with the ^{60}Co radioactive source and the evolution of the 1173.2 and 1332.5 keV transitions was followed. When the compensation circuit was OFF, the temperature variation was done in the interval between 30.1 °C and 33.1 °C. With the compensation ON, the temperature variation was done in the interval between 30 °C and 34.7 °C. In the case of the measurement with no compensation, the energy resolution is degraded as the centroid of the peak has shifted by about 41.5 keV for the 3 °C temperature interval (panel (a)). When acting on the overvoltage with the compensation circuit, the stability of the gain is considerably improved, and the gain shift is reduced to a value of 4.7 keV, although the temperature was varied by 4.7 °C (panel (b)).

5. Conclusions

In conclusion, the comparative analysis of the use of SiPMs and PMTs in conjunction with $LaBr_3$(Ce) crystals for applications of the fast-timing method in γ-ray spectroscopy has provided valuable insights into the performance characteristics, advantages, and limitations of each combination. The SiPM detector has considerably smaller dimensions as compared to the bulky PMT, making possible a closer packing of detectors and increased efficiency. With the current readout electronics, the energy resolution of the SiPM-based detector is found to be better, with values around 10%–15%, as compared to the PMT-based detector, up to energies of about 1.4 MeV. At the same time, the timing response is measured to have a similar value in both cases, around 230 ps FWHM, proving that the SiPM technology is mature enough to replace the PMTs in γ ray spectroscopy. In addition, a temperature compensation circuit was developed and tested. We have shown that temperature variations up to 4.7 °C can be accounted for by the solution we propose, with a gain shift of less than 5 keV for the 1332.5 keV transition. All these characteristics place the FATIMA array in a leading position in the field of fast-timing measurements, allowing its use in nuclear structure experiments at future radioactive beam facilities.

CRediT authorship contribution statement

S. Pascu: Writing – original draft, Validation, Formal analysis, Conceptualization. **A. Stoica:** Validation, Software, Investigation, Conceptualization. **C. Neacşu:** Writing – review & editing, Validation, Methodology, Conceptualization. **A. Bruce:** Writing – review & editing, Resources, Methodology, Funding acquisition. **C. Costache:** Validation, Investigation, Formal analysis, Data curation. **B. Das:** Validation, Investigation, Formal analysis, Data curation. **M. Górska:** Writing – review & editing, Methodology, Investigation, Conceptualization. **C. Mihai:** Writing – review & editing, Methodology, Data curation, Conceptualization. **M. Mikolajczuk:** Validation, Investigation, Formal analysis. **Zs. Podolyák:** Writing – review & editing, Project administration, Funding acquisition, Conceptualization. **P.H. Regan:** Project administration, Funding acquisition, Conceptualization. **A. Turturică:** Validation, Software, Investigation, Formal analysis.

Declaration of competing interest

The authors declare that they have no known competing financial interests or personal relationships that could have appeared to influence the work reported in this paper.

Acknowledgments

This work is supported by the UK STFC under Grants No. ST/V001108/1, ST/Y000358/1, and by the Romanian Ministry for Research and Innovation (MCI), United Kingdom under contract 04FAIR/2020. PHR acknowledges support from the UK National Measurements System Programmes Unit of the UK's Department for Science, Innovation and Technology (DESIT).

Data availability

Data will be made available on request.

References

[1] V. Golovin, 1998, Patent No. RU 2142175.
[2] Z. Sadygov, 1998, Patent No. RU 2102820.
[3] D. Di Vita, L. Buonanno, F. Canclini, G. Ticchi, F. Camera, M. Carminati, C. Fiorini, Nucl. Instrum. Methods Phys. Res. A 1040 (2022) 167179.
[4] M.G. Bisogni, A. Del Guerra, N. Belcari, Nucl. Instrum. Methods Phys. Res. A 926 (2019) 118.
[5] A. Berti, A. Chiavassa, D. Corti, D. Depaoli, F. Di Pierro, L. Lessio, M. Mallamaci, M. Mariotti, C. Perennes, R. Rando, P. Vallania, C. Vigorito, Nucl. Instrum. Methods Phys. Res. A 982 (2020) 164373.
[6] M. Carminati, D. Di Vita, G. Morandi, I. D'Adda, C. Fiorini, Sensors 22 (2022) 1412.
[7] G. Llosá, Nucl. Instrum. Methods Phys. Res. A 926 (2019) 148.
[8] M. Grodzicka-Kobylka, M. Moszyński, T. Szczęśniak, Nucl. Instrum. Methods Phys. Res. A 926 (2019) 129.
[9] H. Mach, R.L. Gill, M. Moszynski, Nucl. Instrum. Methods Phys. Res. A 280 (1989) 49.
[10] M. Moszynski, H. Mach, Nucl. Instrum. Methods Phys. Res. A 277 (1989) 407.
[11] N. Mărginean, et al., Eur. Phys. J. A 46 (2010) 329.
[12] J.M. Regis, et al., Nucl. Instrum. Methods Phys. Res. A 763 (2014) 210.
[13] M. Rudigier, et al., Nucl. Instrum. Methods Phys. Res. A 969 (2020) 163967.
[14] B. Rubio, Int. J. Mod. Phys. E 15 (2006) 1979.
[15] Z. Podolyak, Nucl. Instrum. Methods Phys. Res. A 266 (2008) 4589.
[16] D. Bucurescu, et al., Nucl. Instrum. Methods Phys. Res. A 837 (2016) 1.
[17] S. Alam, et al., Nucl. Instrum. Methods Phys. Res. A 874 (2017) 103.
[18] J.M. Regis, et al., Nucl. Instrum. Methods Phys. Res. A 955 (2020) 163258.
[19] C. Mihai, et al., Nucl. Instrum. Methods Phys. Res. A 953 (2020) 163263.
[20] C. Neacsu, (Ph.D thesis), 2022, unpublished.
[21] https://www.onsemi.com/pdf/datasheet/microj-series-d.pdf.
[22] M. García-Díez, et al., IEEE Trans. Rad. Plasma Med. Sci. 7 (2023) 587.
[23] https://www.eeweb.com/wp-content/uploads/articles-app-notes-files-signal-driven-multiplexing-of-silicon-photomultiplier-arrays.pdf.
[24] https://www.onsemi.com/pub/Collateral/AND9778-D.PDF.
[25] G. Simpson, S. Curtoni, D. Dauvergne, M.-L. Gallin-Martel, S. Marcatilli, G. Thiamova, Nucl. Instrum. Methods Phys. Res. A 940 (2019) 50.
[26] O.J. Roberts, A.M. Bruce, P.H. Regan, Z. Podolyák, C.M. Townsley, J.F. Smith, K.F. Mulholland, A. Smith, Nucl. Instrum. Methods Phys. Res. A 784 (2014) 91.
[27] A.N. Otte, D. Garcia, T. Nguyen, D. Purushotham, Nucl. Instrum. Methods Phys. Res. A 846 (2017) 106.